

Journal of Al-Azhar University Engineering Sector



Vol. 20, No. 77, October 2025, 1125-1142

EFFECT OF 3D INCLINATION ANGLES ON DISCHARGE COEFFICIENT FOR WATER FLOW THROUGH REGULAR POLYGONAL MULTI-ORIFICE EXITS

Ahmed M. Abdelrahman 1*, Anas M. Elmolla 2,3, Amir M. Mobasher 2,4

- ¹ Civil Engineering Department, Canadian International College (CIC), Cairo, Egypt
- ² Civil Engineering Department, Faculty of Engineering, Al-Azhar University, Cairo, Egypt
- 3 Civil Engineering Department, Faculty of Engineering, Galala University, Galala, Egypt
- ⁴ Civil Engineering Department, Madina Higher Institute for Engineering and Technology, Cairo, Egypt
 - * Correspondence: ahmed_m_abdelrahman@cic-cairo.com

Cita**ti**on:

A. M. Abdelrahman, A. M. Elmolla, A. M. Mobasher, "Effect of 3D Inclination Angles on Discharge Coefficient for Water Flow through Regular Polygonal Multi-Orifice Exits," Journal of Al-Azhar University Engineering Sector, vol. 20, No. 77, pp. 1125-1142, 2025.

Received: 22 January 2025 Revised: 03 April 2025 Accepted: 29 June 2025

Doi: 10.21608/auej.2025.354398.1760

Copyright © 2025 by the authors. This article is an open access article distributed under the terms and conditions Creative Commons Attribution-Share Alike 4.0 International Public License (CC BY-SA 4.0)

ABSTRACT

The discharge coefficient (C_d) is a fundamental parameter in multi-orifice flow, critical for hydraulic systems and flow control applications. This study examines how three-dimensional inclination angles affect Cd for water flow through multiorifice exits. Using Buckingham's π -Theorem, we conducted dimensional analysis to identify key dimensionless parameters influencing C_d. We performed both experimental tests and computational fluid dynamics (CFD) simulations to evaluate how geometric parameters including inclination angles of multi-orifices in the flow direction and perpendicular to it impact performance. The analysis included five orifice shapes: circular, triangular, square, pentagonal, and hexagonal, with numerical extensions exploring additional polygonal configurations. Results show that the discharge coefficient exhibits distinct patterns under two rotation conditions. When rotated about the flow direction axis, C_d oscillates periodically, decreasing to 94% of its original value with a 6% amplitude. These systematic variations are influenced by both the rotation angle θ_1 and the number of polygon sides (m). When rotated about the perpendicular axis by angle θ_2 , C_d oscillates consistently across all tested geometries, decreasing to 92% of its original value with an 8% amplitude. The measured C_d values range from 0.635 to 0.716. These findings establish quantitative relationships between geometric orientation and discharge efficiency in multiorifice systems.

KEYWORDS: Discharge coefficient, multi-orifice flow, dimensional analysis, periodic variation, CFD simulation

تأثير زوايا الميل ثلاثية الأبعاد على معامل التصرف لتدفق المياه عبر المخارج متعدة الفوهات ذات الأشكال المضلعة المنتظمة

أحمد محمود عبد الرحمن عبد المنعم ١*، أنس محمد أبو العلا الملا ٢٠١ ، أمير محمد عقل عباس مباشر ٢٠٠

ا قسم الهندسة المدنية، الكلية الكندية الدولية، القاهرة، مصر القسم الهندسة المدنية، كلية الهندسة، جامعة الأزهر، القاهرة، مصر تقسم الهندسة المدنية، كلية الهندسة، جامعة الجلالة، الجلالة، مصر قسم الهندسة المدنية، معهد المدينة العالي للهندسة والتكنولوجيا، القاهرة، مصر

* البريد الإلكتروني للباحث الرئيسي: hmed m abdelrahman@cic-cairo.com

الملخص

معامل التصرف هو أحد المعاملات الأساسية في تدفق السوائل عبر الفتحات المتعددة، حيث يلعب دورًا محوريًا في الأنظمة الهيدروليكية وتطبيقات التحكم في التندفق. تدرس هذه الدراسة تأثير زوايا الميل ثلاثية الأبعاد على معامل التصرف لتدفق المياه عبر مخارج متعددة الفتحات. تم إجراء تحليل بعدي باستخدام نظرية باكنغهام لتحديد المعاملات اللابعدية الرئيسية الموثرة على معامل التصرف. كما تم إجراء كل من الاختبارات المعملية ومحاكاة ديناميكا الموائع الحسابية لتقييم تأثير العوامل الهندسية، بما في ذلك زوايا ميل الفتحات المتعددة في اتجاه الندفق والاتجاه العمودي عليه. شمل التحليل خمسة أشكال للفتحات: الدائرية، والمربعة، والمحربعة، والخماسية، والسداسية، بالإضافة إلى توسعات عدية لاستكشاف فتحات متعددة بأشكال مضلعة إضافية أظهرت النتائج أن معامل التصرف يتغير بشكل ملحوظ تحت حالتين من الدوران. عند الدوران حول محور التدفق، يتذبذب معامل التصرف بشكل دوري، حيث يصل إلى حد أدنى يعادل ٩٤٪ من قيمته الأصلية، مع سعة تذبذب تبلغ ٨٪. وتتراوح قيم معامل التصرف المقاسة بين ٥٣٠، و ٢١٠، تقدم هذه النتائج علاقات كمية تربط بين التوجيه قيمته الأصلية، مع سعة تذبذب تبلغ ٨٪. وتتراوح قيم معامل التصرف المقاسة بين ٥٣٠، و ٢١٠، تقدم هذه النتائج علاقات كمية تربط بين التوجيه الهندسي وكفاءة التصريف في أنظمة الفتحات المتعددة.

الكلمات المفتاحية : معامل التصريف، تدفق متعدد الفتحات، التحليل البعدي، التغير الدوري، محاكاة ديناميكا الموانع الحسابية.

INTRODUCTION

Inclined multi-orifice exits play a crucial role in various industrial processes that require precise mixing and dispersion. In fields such as chemical processing and water treatment, these configurations enhance coagulation and flocculation efficiency by generating controlled turbulence patterns. The ability to manipulate discharge characteristics by adjusting orifice inclination offers precise control over fluid interactions, which is particularly beneficial in mineral processing and pharmaceutical manufacturing. Additionally, these systems are becoming increasingly important in energy generation, including hydroelectric plants, where precise flow control is essential for maximizing operational efficiency. Multi-orifice exits are also commonly used in agricultural irrigation systems, helping to distribute water uniformly across cultivated areas, thereby improving water efficiency and minimizing losses [1]. Due to their versatility and broad range of applications, these systems have inspired numerous empirical and computational studies aimed at understanding flow behavior through multi-orifice configurations.

For example, the flow characteristics of 16 orifices with varying beta ratios were investigated, where multi-hole orifices (MHO) were compared to single-hole orifices (SHO). The results demonstrated that MHOs achieved higher discharge coefficients and reduced pressure loss coefficients by 30.81% to 32.57%, indicating superior hydraulic performance [2]. This finding underscores MHO's potential as an effective alternative to traditional SHO configurations. Similarly, the advantages of multi-hole orifice plates over single-hole plates in terms of performance were highlighted [3]. This observation was consistent with earlier studies, where the discharge coefficients of standard single orifices were compared with those of perforated orifices

at low Reynolds numbers. It was shown that perforated orifices delivered discharge coefficients that were 22.5% to 25.6% higher than those of standard single orifices [4].

Accurate prediction of the discharge coefficient is essential for designing hydraulic systems. It was reported that the discharge coefficient decreases with an increase in the orifice-to-pipe diameter ratio and the head-to-crest height ratio, while the orifice crest height-to-orifice height ratio was identified as a key influencing factor [5].

Expanding on these findings, experimental studies on multi-orifice flow within a hydraulic measuring flume with a constriction factor of $\beta = 0.5$ showed that tests performed at Reynolds numbers ranging from 4700 to 19,500 demonstrated a consistent discharge coefficient of 0.6286, which was approximately 2% higher than that of a centrally placed single orifice with an equivalent constriction [6]. Similar results were later corroborated [7].

It was found that a 25-hole orifice plate yielded a 24.2% higher discharge coefficient compared to a single-hole orifice [8]. Moreover, increasing the beta ratio (β) was shown to reduce pressure drop and improve the discharge coefficient for Re = 105 at β values of 0.55, 0.6, and 0.7 [9]. In addition, triangular orifices were identified as offering the highest discharge coefficient (0.62–0.8) and lowest head loss, while Reynolds number had little effect above 5000 [10]. Furthermore, MLR and MNLR models were developed to predict the discharge coefficient of triangular side orifices with accuracies within $\pm 5\%$ and $\pm 12\%$ of experimental values using 570 data sets [11].

In summary, no existing studies comprehensively investigate the combined effects of 3D inclination angles and geometric orientation on discharge characteristics across polygonal multi-orifice configurations. While previous studies have focused on single-orifice shapes or limited geometries, the effects of 3D inclination and geometric orientation have remained underexplored. This research addresses this critical knowledge gap by establishing quantitative relationships between rotation angles, geometric parameters, and discharge coefficients, which will advance fundamental understanding of multi-orifice flow systems. Such insights can guide more efficient design and optimization of multi-orifice systems in various industrial applications.

DIMENSIONAL ANALYSIS AND PHYSICAL MODELING

In this study, we apply dimensional analysis to investigate flow behavior through multi-orifice exits. The traditional approach begins with discharge as a function of relevant parameters:

$$Q = f(\rho, v, d, \mu, h, t, g, k, n, m, \theta_1, \theta_2)$$
 Eq. 1

According to Buckingham's π -Theorem, with 13 variables and 3 fundamental dimensions (M, L, T), we can form 10 dimensionless groups. Selecting ρ , g, and d as repeating variables, we form the dimensionless group for discharge Q:

$$\pi_1 = \rho^a. g^b. d^c. Q$$
 Eq. 2

Solving for dimensionless conditions yields a = 0, b = -1/2, c = -2, resulting in:

$$\pi_1 = \frac{Q}{d^2 / \sqrt{gh}}$$
 Eq. 3

This dimensionless group is proportional to the discharge coefficient C_d , which represents the ratio of actual to theoretical discharge:

$$C_d = \frac{Q}{A/\sqrt{2gh}} \propto \frac{Q}{d^2/\sqrt{gh}}$$
 Eq. 4

Through similar analysis of other parameters, we obtain:

$$C_d = f\left(\frac{h}{d}, \frac{t}{d}, \frac{v}{\sqrt{gh}}, \frac{\mu}{\rho h \sqrt{gh}}, k, n, m, \theta_1, \theta_2\right)$$
 Eq. 5

For our experimental conditions with constant fluid properties and geometric ratios, this reduces to:

$$C_d = f(k_1 n_1 m_1 \theta_1, \theta_2)$$
 Eq. 6

This analysis enables us to isolate and study how shape factor, number of orifices, number of sides, and 3D inclination angles influence the discharge coefficient in multi-orifice systems.

The experimental apparatus utilized a modified version of a previously fabricated model, optimized for this investigation. The setup consists of two primary components: an upper tank and a lower tank (**Fig. 1**), both constructed from 5 mm transparent acrylic sheets. The acrylic material was selected for its compatibility with laser cutting technology and optical transparency, which enabled precise fabrication and clear visualization of flow patterns.

The lower tank functions as a collecting reservoir for water discharged through the multi-orifice exits and facilitates water recirculation. A 0.25 hp centrifugal pump was incorporated into the system to transport water from the lower tank to the upper tank. The upper tank was specifically designed to maintain a constant hydraulic head above the orifice plates during testing.

Head control was achieved with a concentric pipe arrangement installed at the upper tank's center. This system includes a fixed inner pipe installed at the bottom of the tank and an adjustable outer pipe. The outer pipe's vertical position can be adjusted to precisely regulate the water head above the multi-orifice plates. **Fig. 2** provides photographic documentation of the experimental setup, including the model assembly and the various orifice plates used in the investigation.

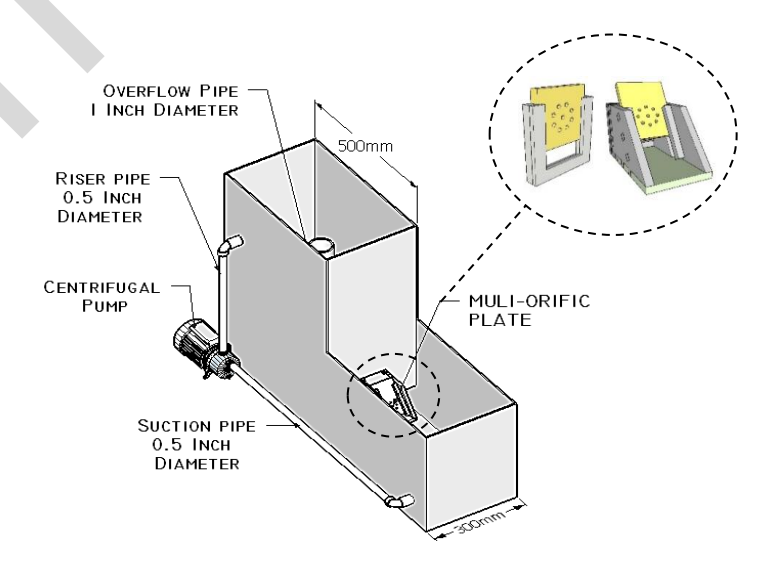


Fig. 1: Model isometric definition sketch.



Fig. 2: Real photo of the physical model and orifice plates

The discharge coefficient was determined by measuring the volume of water discharged through the multi-orifice exit over a specific time interval. The discharged volume was collected in an external graduated vessel, allowing precise volume measurement. The flow rate was then calculated by dividing the collected volume by the elapsed time.

EXPERIMENTAL AND CFD WORKS:

1.1. EXPERIMENTAL SETUP AND DISCHARGE CALCULATION

To explore the effects of 3D orientation angles on multi-orifice flow characteristics, a set of 36 orifice plates was carefully fabricated using precision laser technology from 10 mm thick transparent acrylic sheets. The experiments comprised 16 plates for θ_1 testing (rotation about the X-Z plane: 0° , 15° , 30° , and 45°) and 20 plates for θ_2 testing (rotation about the Y-Z axes: 0° , 20° , 40° , and 60°). For θ_1 analysis, four polygonal configurations (triangular, square, pentagonal, and hexagonal) were examined, excluding circular geometry due to its symmetry in the Y-Z plane. For θ_2 analysis, all five geometric configurations were tested. The base plate dimensions (70 mm × 70 mm) were scaled to accommodate angular orientations: 70 mm × 82.8 mm (15°), 70 mm × 92.4 mm (30°), and 70 mm × 113.1 mm (45°). Precision grooves were added into the design to ensure accurate plate positioning and facilitate systematic testing procedures. **Fig. 3** and **Fig. 4** show the orifice configurations.

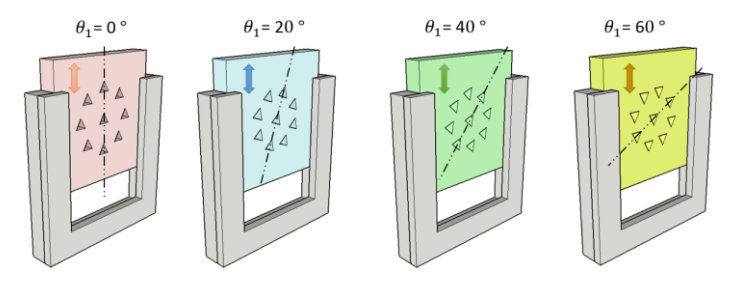


Fig. 3: Orifice plate installation for different angles in X-Y plane.

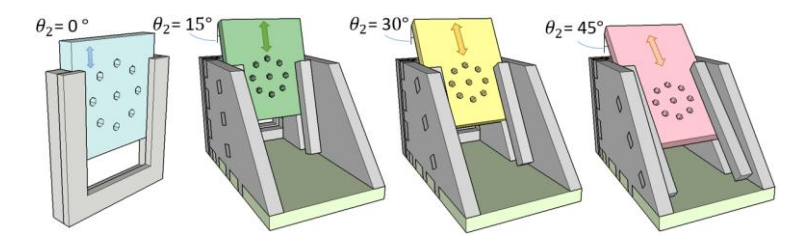


Fig. 4: Orifice plate installation for different angles in X-Z plane.

To measure the discharge from the multi-orifice plates, water was allowed to flow through the orifices while the elapsed time was measured using a stopwatch. After the designated time period, the orifice was closed, and the drained water was collected in an external graduated vessel to measure the volume (**Fig. 2**). The actual discharge was then calculated using the relationship:

$$Q_{ex} = \frac{dV}{dt}$$
 Eq. 7

Where Q_{ex} is the experimentally measured discharge, dV is the volume of collected water, and dt is the recorded time. To clarify how the discharge coefficient C_d was determined, the experimental parameters were categorized into input, output, and derived parameters, as shown in the following (**Table 1**).

Table 1. Detailed experimental parameters for discharge measurement.

Parameter Category	Parameter	Value	Description
Input Parameters	Inclination Angle (θ 1)	0°, 15°, 30°, and 45°	Orifices rotation about the X-Z plane
	Inclination Angle (θ 2)	0°, 20°, 40°, and 60°	Orifices rotation about the Y-Z plane
	Plate Geometry	Circular, Triangular, Square, Pentagonal, Hexagonal	Changing the number of sides of regular polygons.
	Water Head (h)	500 mm	Initial water height in the reservoir
	Orifice Diameter (d)	5 mm	Diameter for circular or equivalent diameter for non-circular shapes
	Multi-Orifice Area (A)	176.7 mm²	Sum of all individual orifice areas
4	Orifice Thickness (t)	10 mm	Thickness of the acrylic plate
	Spacing between orifices (S)	15 mm	Distance from the centroid of a circumferential orifice to the group center
	Number of orifices (n)	9 orifices	Total number of orifices per plate
Output Parameters	Elapsed Time (t)	Varies per run	Time taken to collect the discharged volume
	Collected Volume (V)		Volume of water discharged through the orifices
Derived Parameters	Experimental Discharge (Q _{ex})	Varies per run	Measured discharge based on collected volume and elapsed time
	Theoretical Discharge (Q _{th})		Calculated as $Qth=A2ghQ_{th} = A$ $\sqrt{2gh}Qth=A2gh$
	Discharge Coefficient (C _d)		Ratio of actual discharge to theoretical discharge

Table 2 provides a detailed sample calculation of the discharge coefficient for nine pentagonal orifices, illustrating both theoretical and experimental discharge values. The discharge coefficient is determined by dividing the experimental discharge by the theoretical discharge.

Table 2. Sample discharge calculation for nine pentagonal orifices (d = 5 mm, s = 15 mm, h = 50 cm, θ 1 = 20°, θ 2 = 0°)

Orifice	Theoretical Discharge			Experimental Discharge			Cd	Orifice	
Serial	(h) (cm.)	Velocity $v = \sqrt{2gh}$ (cm/s)	(Q_{th}) $Q_{th} = Av$ (cm^3/s)	Averag e (Qth) (cm³/s)	Volume (cm ³)	Time (s)	(Qex) dV/dt (cm ³ /s)		Configuration
Orifice 1	٥٠,٠٠	۳۱۳,۲۰ 9	71,£9.	٥٥٣,٣٨١	1493	4.17	358.034	0.647	
Orifice 2	0.,01	٣١٤,٨٠٣	71,4.4	-					5 4
Orifice 3	٤٩,٣٧	T11,7T+	71,111	-					6 3
Orifice 4	٤٨,٥٩	۳۰۸,۷٦١	٦٠,٦١٧	-					7 2
Orifice 5	٤٨,٦٤	۳۰۸,۹۲۰	٦٠,٦٤٨	-					8 9
Orifice 6	٤٩,٤٩	۳۱۱,٦٠٨	71,170	-				Ť	
Orifice 7	٥٠,٦٣	٣١٥,١٧٦	٦١,٨٧٦	-					
Orifice 8	01, £1	T1V,090	77,701	-					
Orifice 9	01,77	٣١٧, ٤٤٠	٦٢,٣٢٠	-					

1.2. NUMERICAL MODEL

Computational fluid dynamics (CFD) modeling was used to simulate water flow through multiorifices, with the goals of validating experimental results. Autodesk CFD 2021 was employed for simulations, utilizing its built-in solver, meshing tool, and SIMPLE algorithm. A fine cubic mesh (0.1 cm) was applied to the multi-orifice plate and the critical flow region (0.5 cm ahead); while a coarser mesh, (0.2 cm) was used farther from the orifices, as shown in **Fig. 5**.

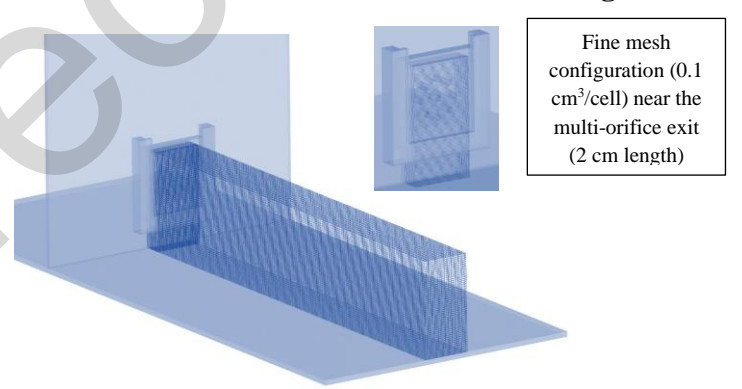


Fig. 5: Mesh representation of multi-orifice exit in isometric perspective (50 cm length).

1.3. MATHEMATICAL MODEL

The purpose of this section is to establish a mathematical representation of the rotational effect on the discharge coefficient C_d based on its inherent periodic nature. Since rotation follows a periodic pattern, the variations in C_d are expected to exhibit cyclical behavior. To accurately capture this effect, trigonometric functions, specifically the cosine function, are used, as they inherently describe periodic oscillations.

The proposed model expresses the percentage change in C_d through periodic equations. The percentage change in C_d at a given inclination angle relative to its value at zero inclination is defined as follows:

For rotation about the X-axis (the flow direction axis):

$$P_1 = a_1 + b_1 \cos(q_1 \theta_1)$$
 Eq. 8

For rotation about the Y-axis (the axis perpendicular to the flow direction):

$$P_2 = a_2 + b_2 \cos(q_2 \theta_2)$$
 Eq. 9

The use of the cosine function is based on the assumption that changes in C_d due to inclination angles follow a periodic trend. This periodic behavior arises because the inclination alters the effective flow area and flow resistance in a cyclic manner. This mathematical framework systematically quantifies these rotational effects, providing a structured approach to evaluate the influence of inclination angles on C_d before presenting the results. The subsequent analysis determines these characteristic parameters.

Where P_1 and P_2 represent the percentage change in C_d due to inclination about the X and Y axes, respectively. The terms a1 and a_2 denote the mean percentage changes in C_d , while b_1 and b_2 represent the oscillation amplitudes, capturing variations around the mean value. Finally, q_1 and q_2 are periodicity coefficients that define the frequency of oscillations.

1.4. EXPERIMENTAL PROGRAM

The experimental program aimed to investigate the effect of inclination angles on the discharge coefficient C_d and establish mathematical relationships between the inclination angles θ_1 around the X-axis and θ_2 around the Y-axis) and C_d . To achieve this, the orifices were tested at specific inclination angles: θ_1 at 0° , 20° , 0° , and 60° , and θ_2 at 0° , 15° , 30° , and 45° . All orifice shapes were designed with an equal area of about 19.63 mm² (equivalent to the area of a circular orifice with a 5 mm diameter) to ensure consistent flow comparison across different geometries. All other parameters were kept constant, as presented in **Table 1**, to ensure accurate measurements and isolate the effect of inclination on flow behavior.

The experiments began by setting up the hydraulic system according to the previously described model, ensuring a stable water level in the upper tank. After adjusting the orifice plate to the desired inclination angle, the flow was initiated, allowing water to pass through the multi-orifice exits. The actual discharge (Q_{exp}) was measured by collecting the discharged water in an external graduated vessel over a specific time period, which was recorded using a stopwatch. The actual discharge was then calculated using the equation: dV/dt.

Simultaneously, the theoretical discharge Q_{th} was determined using Bernoulli's equation, which considers the pressure difference driving the flow through the orifices:

$$Q_{th} = A\sqrt{2gh}$$
 Eq. 10

where A is the total orifice area, and h is the hydraulic head above the orifice plate. Finally, the discharge coefficient (C_d) was alculated by comparing the actual and theoretical discharge values using the following equation:

$$C_d = \frac{Q_{ex}}{Q_{th}}$$
 Eq. 11

A sample discharge calculation following these steps is explained in the experimental setup and discharge calculation section, showing how C_d is determined using measured and theoretical discharge values.

This process was repeated for each inclination angle to thoroughly analyze its effect on the discharge coefficient and assess how well the results align with the proposed mathematical model.

RESULTS AND DISCUSSION

1.5. COMPARATIVE EXPERIMENTAL AND CFD RESULTS

For both directions, the experimental data are presented in a table containing the discharge coefficients of the five multi-orifice shapes (circular, equilateral triangular, square, pentagonal, and hexagonal) and the inclination angles. The relationship between angles and C_d was analyzed by plotting angles as independent variables and C_d as dependent variable.

For θ_1 , the experimental results were verified numerically using CFD (**Fig. 6**), and the results were presented alongside the experimental results (**Table 3**). The comparison between the experimental and numerical results is shown in **Fig. 7** where the upper graph displays the laboratory results, followed by individual graphs for each orifice shape incorporating both the experimental and numerical results. Additionally, the percentages of the difference between the two sets of results for each record are indicated on the graphs and listed in **Table 3**.

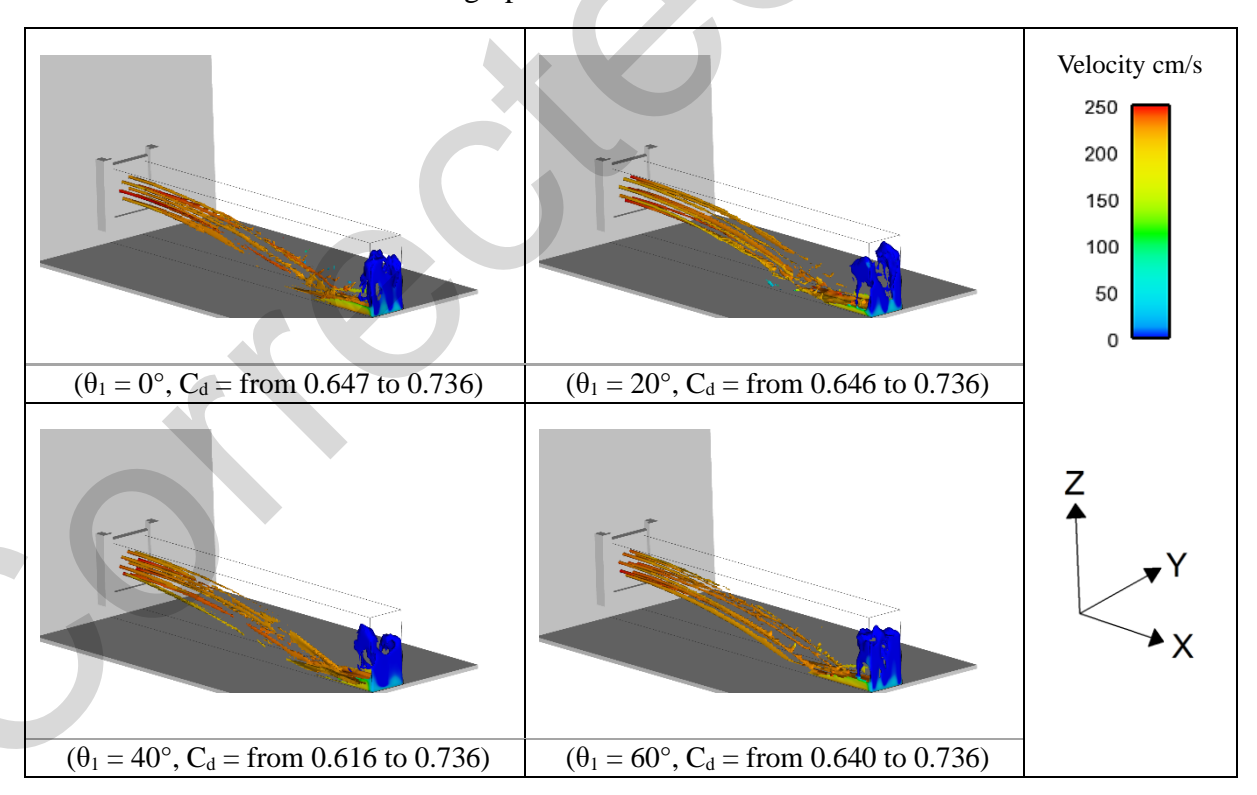


Fig. 6: Samples of numerical C_d simulation vs. rotation angle θ_1 .

Table 3. Experimental vs. CFD comparison of multi-orifice C_d at varying rotation angle θ_1 .

θ1	Multi- Orifice Shape	Coefficient of Di	Difference (%)	
		Experimental	CFD	
0°	Circular Orifices	0.716	0.736	2.8%
	Equilateral Triangular Orifices	0.697	0.716	2.7%
	Square Orifices	0.684	0.692	1.2%
	Pentagonal Orifices	0.670	0.647	-3.4%
	Hexagonal Orifices	0.664	0.676	1.8%
20 °	Circular Orifices	0.716	0.736	2.8%
	Equilateral Triangular Orifices	0.685	0.702	2.5%
	Square Orifices	0.666	0.646	-3.0%
	Pentagonal Orifices	0.647	0.667	3.1%
	Hexagonal Orifices	0.637	0.665	4.4%
40°	Circular Orifices	0.716	0.736	2.8%
	Equilateral Triangular Orifices	0.667	0.675	1.2%
	Square Orifices	0.645	0.616	-4.5%
	Pentagonal Orifices	0.635	0.630	-0.8%
	Hexagonal Orifices	0.637	0.620	-2.7%
60°	Circular Orifices	0.716	0.736	2.8%
	Equilateral Triangular Orifices	0.655	0.640	-2.3%
	Square Orifices	0.649	0.624	-3.9%
	Pentagonal Orifices	0.663	0.657	-0.9%
	Hexagonal Orifices	0.662	0.633	-4.4%

For θ_2 , the experimental results were similarly verified numerically using CFD (**Fig 8**), and both results were presented alongside each other (**Table 4**). The comparison between the experimental and numerical results is shown in **Fig. 9**, where the upper graph displays the laboratory results, followed by individual graphs for each orifice shape incorporating both result sets. The percentage differences between the two sets of results for each record were also indicated on the graphs and listed in **Table 4**.

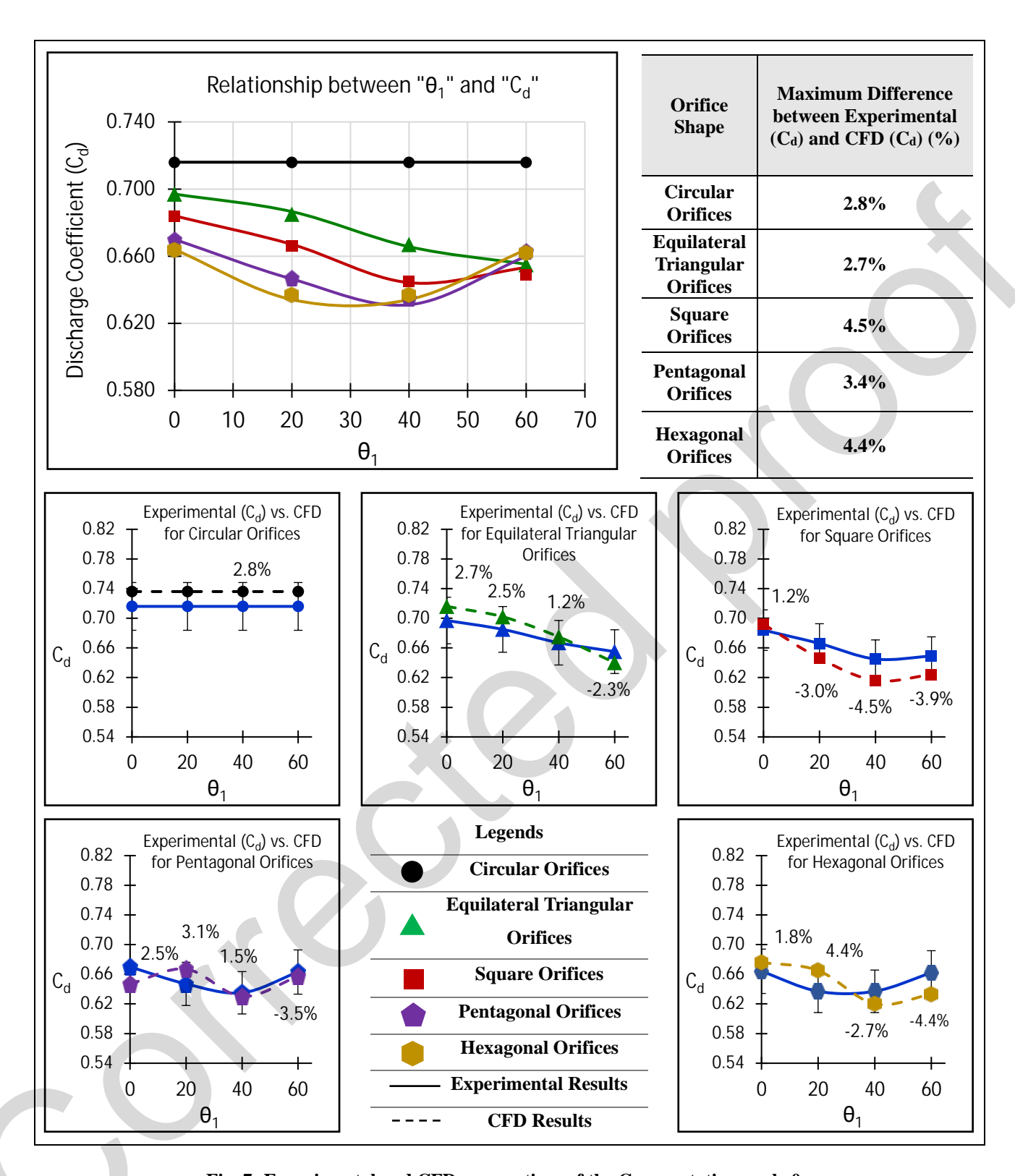


Fig. 7: Experimental and CFD perspectives of the C_d vs. rotation angle θ_1 .

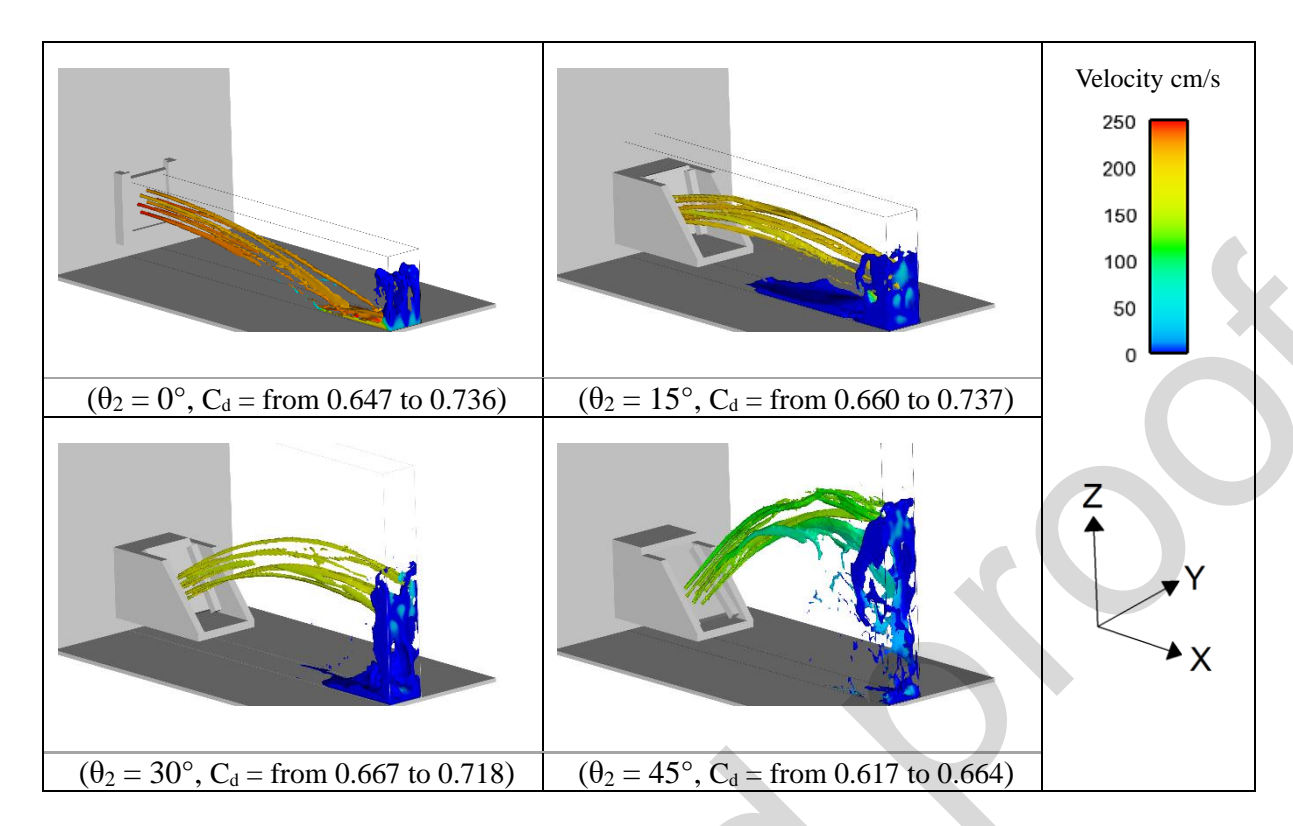


Fig 8: Samples of numerical C_d simulation vs. rotation angle θ_2 .

Table 4. Experimental vs. CFD comparison of multi-orifice C_d at varying rotation angle θ_2 .

θ_2	Multi- Orifice Shape Coefficient of Discharge (C _d)			Difference (%)
	X	Experimental	CFD	_
0 °	Circular Orifices	0.716	0.736	2.8%
	Equilateral Triangular Orifices	0.697	0.716	2.7%
	Square Orifices	0.684	0.692	1.2%
	Pentagonal Orifices	0.670	0.647	-3.4%
	Hexagonal Orifices	0.664	0.676	1.8%
15°	Circular Orifices	0.714	0.737	3.2%
	Equilateral Triangular Orifices	0.692	0.703	1.6%
	Square Orifices	0.681	0.660	-3.1%
	Pentagonal Orifices	0.666	0.671	0.8%
	Hexagonal Orifices	0.660	0.666	0.9%
30°	Circular Orifices	0.701	0.718	2.4%
	Equilateral Triangular Orifices	0.682	0.675	-1.0%
	Square Orifices	0.668	0.667	-0.1%
	Pentagonal Orifices	0.655	0.670	2.3%
	Hexagonal Orifices	0.652	0.680	4.3%
45°	Circular Orifices	0.689	0.664	-3.6%
	Equilateral Triangular Orifices	0.669	0.643	-3.9%
	Square Orifices	0.656	0.651	-0.8%
	Pentagonal Orifices	0.644	0.617	-4.2%
	Hexagonal Orifices	0.636	0.661	3.9%

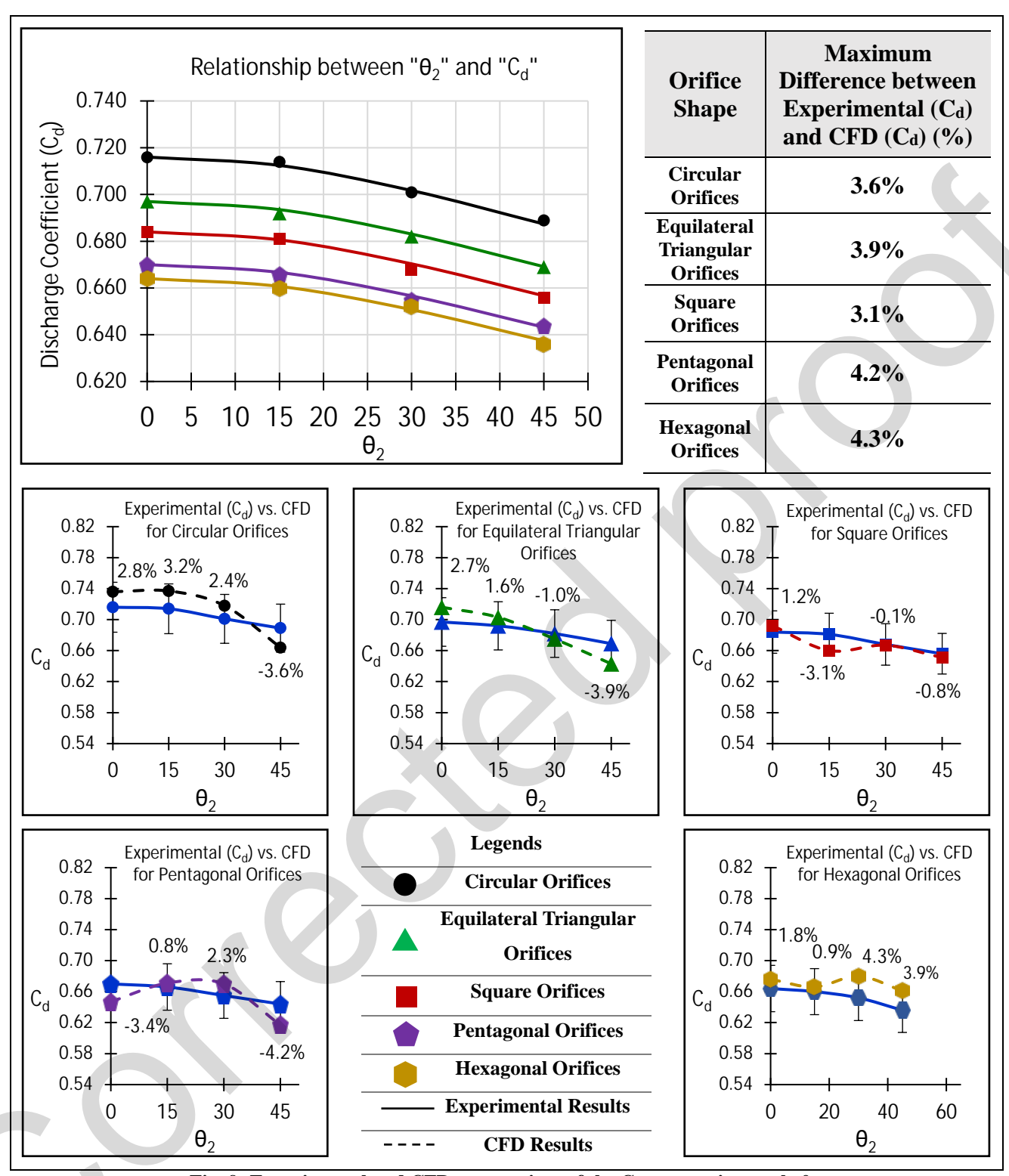


Fig. 9: Experimental and CFD perspectives of the C_d vs. rotation angle θ_2 .

1.6. EVALUATION OF RESULTS

The relationship between the discharge coefficient (C_d) and rotation angle (θ_1) was investigated for non-circular shapes, which remain unaffected due to their supersymmetric properties. The results demonstrated that C_d decreases with increasing θ_1 , with the minimum C_d detected at larger θ_1 values, as shown in **Fig.7**. CFD simulations demonstrated strong agreement with experimental data, with maximum discrepancies of 4.5%. This supports the use of the CFD model to obtain results for

additional runs beyond the limits of the experiments, enabling the derivation of further mathematical equations.

The discharge coefficients (C_d) for non-circular shapes showed a declining trend with increasing rotation angles (θ_1). Experimentally, C_d values ranged from 0.635 to 0.716 for circular orifices, 0.637 to 0.685 for equilateral triangular orifices, 0.616 to 0.684 for square orifices, 0.630 to 0.670 for pentagonal orifices, and 0.620 to 0.676 for hexagonal orifices. The highest observed C_d was 0.736 for circular orifices in CFD simulations.

A similar trend was observed for rotation angles (θ_2), with Cd values declining as the angles increased. Experimentally, Cd values ranged from 0.716 to 0.689 for circular orifices, 0.697 to 0.669 for equilateral triangular orifices, 0.684 to 0.656 for square orifices, 0.670 to 0.644 for pentagonal orifices, and 0.664 to 0.636 for hexagonal orifices. The highest observed Cd for θ_2 was 0.737 for circular orifices in CFD simulations. The reduction in C_d was then quantified as a percentage, denoted by P_1 , relative to the vertical orientation angle (θ_1) in (X–X plane), which varies depending on the polygon type. Each shape requires a specific rotation angle to return to its original position due to its geometric symmetry: 120° for equilateral triangles, 90° for squares, 72° for pentagons, and 60° for hexagons, corresponding to their respective interior angles. Consequently, the number of polygon sides directly influences the mathematical representation of the relationship between θ_1 and C_d . P_1 is defined as the percentage of the discharge coefficient at any angle θ_1 relative to C_d at the vertical position ($\theta_1 = 0^\circ$) **Table 5**.

Equilateral Triangular Pentagonal Hexagonal θ_1 **Square Orifices Orifices Orifices Orifices** 0° (vertical position) 100.00% 100.00% 100.00% 100.00% 20° 97.52% 98.50% 96.48% 95.50% **40**° 95.50% 94.18% 94.18% 95.50% 60° 94.00% 95.50% 98.50% 100.00%

Table 5. Percentage of the discharge coefficient (P₁) with respect to the vertical position.

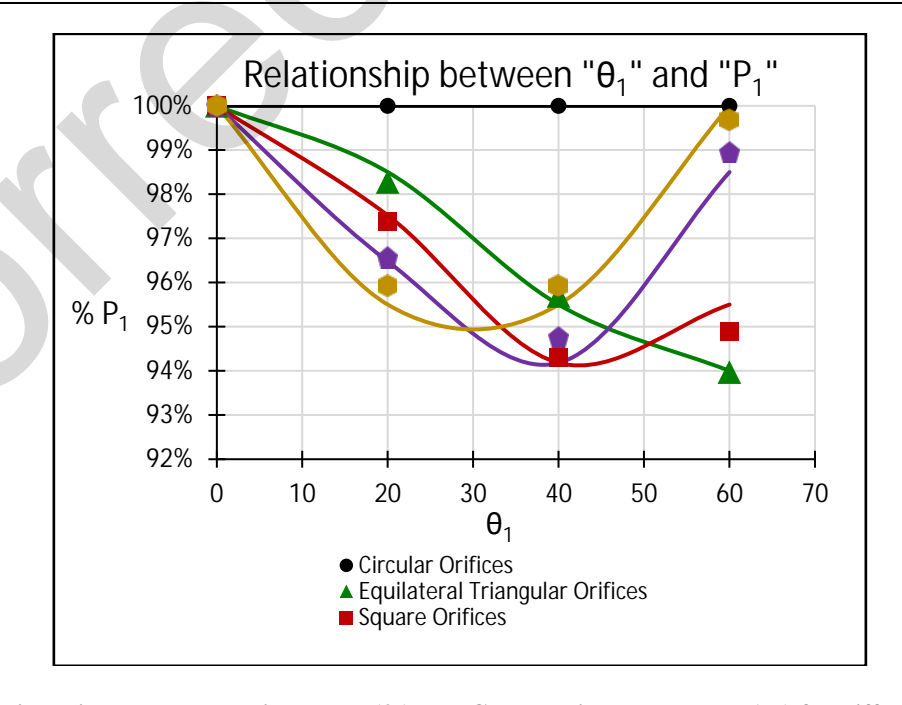


Fig. 10: Relationship between rotation angle (θ_1) and C_d reduction percentage (P_1) for different polygonal shapes.

The values of (P_1) oscillate around a maximum value of 94%, and varies by a maximum of 6%. This value varies based on the angle θ_1 and the number of polygon sides (m) so a typical equation to describe the relationship between the angle (θ_1) and the percentage (P_1) is as follows:

For equilateral triangular orifices:	$P_1 = 0.97 + 0.03\cos(3\theta_1)$	Eq. 12
For square orifices:	$P_1 = 0.97 + 0.03 \cos(4\theta_1)$	Eq. 13
For pentagonal orifices:	$P_1 = 0.97 + 0.03 \cos(5\theta_1)$	Eq. 14
For hexagonal orifices:	$P_1 = 0.97 + 0.03 \cos(6\theta_1)$	Eq. 15

The above equations can be generalized into one general form as follows:

$$P_1 = 0.97 + 0.03 \cos(m\theta_1)$$
 Eq. 16
$$\lim_{\cos(m\theta_1)\to -1} (P_1) = 0.94$$
 Eq. 17
$$\lim_{\cos(m\theta_1)\to 1} (P_1) = 1, \text{ where } P_1 \in [0.94, 1]$$
 Eq. 18

Fig. 11 Illustrates the extension of the curves for all the tested multi-orifice shapes, completing a full cycle with a 360-degree angle.

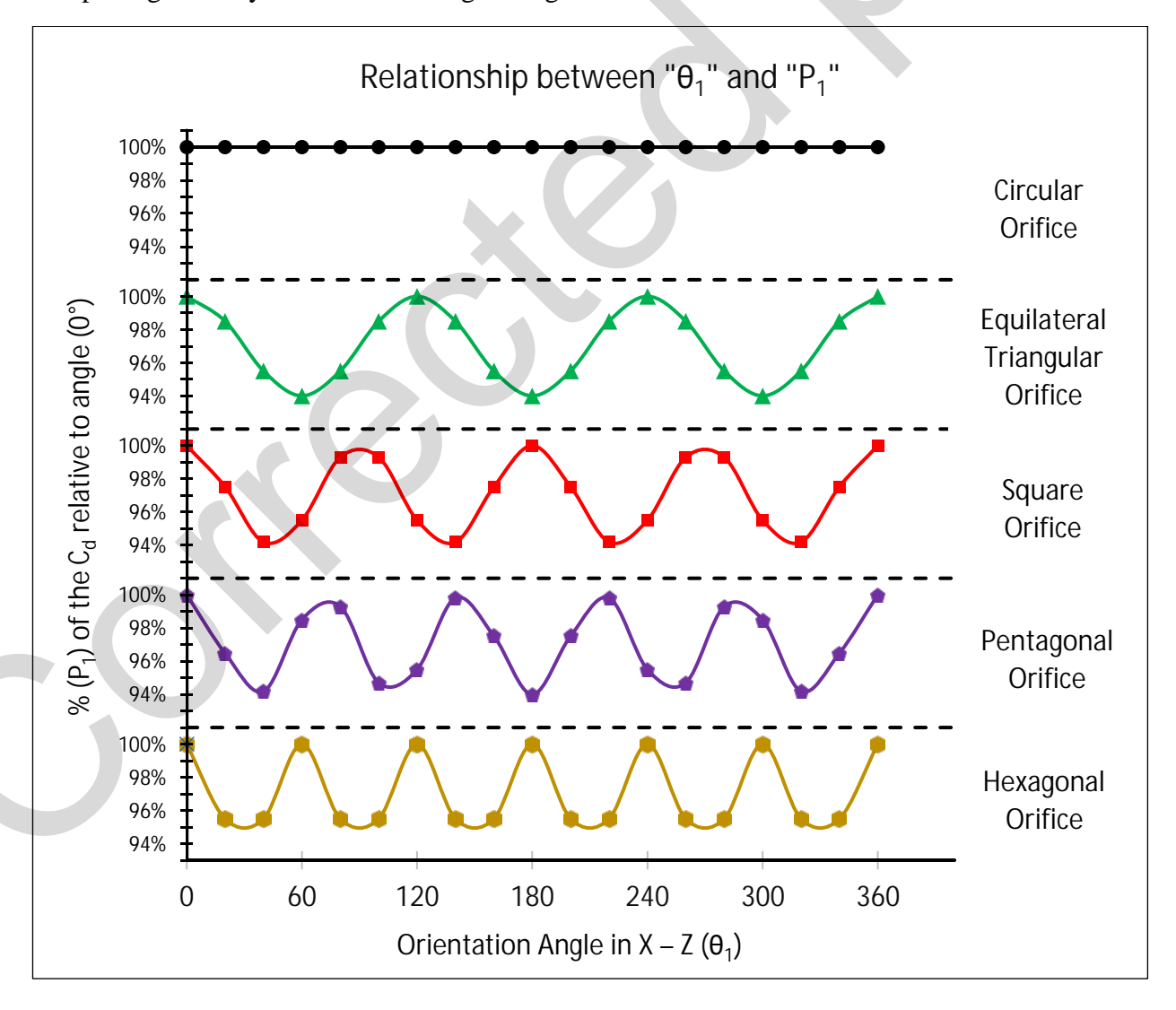


Fig. 11: Extended relationship between θ_1 and C_d reduction (P_1)

The reduction in C_d was then quantified as a percentage, denoted by P_2 , relative to the vertical orientation angle (θ_2) . From the previous experimental results, it appears that the discharge coefficient decreases slightly with alternating the inclination angle (θ_2) in the flow direction (X-Z) plane). By extrapolating the results, we find that the rates of change are almost similar for all shapes. Therefore, P_2 is defined as the percentage of the discharge coefficient at any angle θ_2 relative to C_d at the vertical position $(\theta_2 = 0^\circ)$, meaning that coefficient of discharge at angle (0°) would be considered 100% as shown in **Table 6**.

The most suitable representation of angle variation is trigonometric functions due to their cyclic nature. The cosine function seems to be suitable for this data plot because it starts at 1 and repeats itself every 2π radians, or 360 degrees.

$ heta_2$	Circular Orifices	Equilateral Triangular Orifices	Square Orifices	Pentagonal Orifices	Hexagonal Orifices
0° (vertical position)	100.00%	100.00%	100.00%	100.00%	100.00%
15°	99.72%	99.28%	99.56%	99.40%	99.40%
30°	97.91%	97.85%	97.66%	97.76%	98.19%
45°	96.23%	95.98%	95.91%	96.12%	95.78%

Table 6. Percentage of the discharge coefficient (P2) with respect to the vertical position.

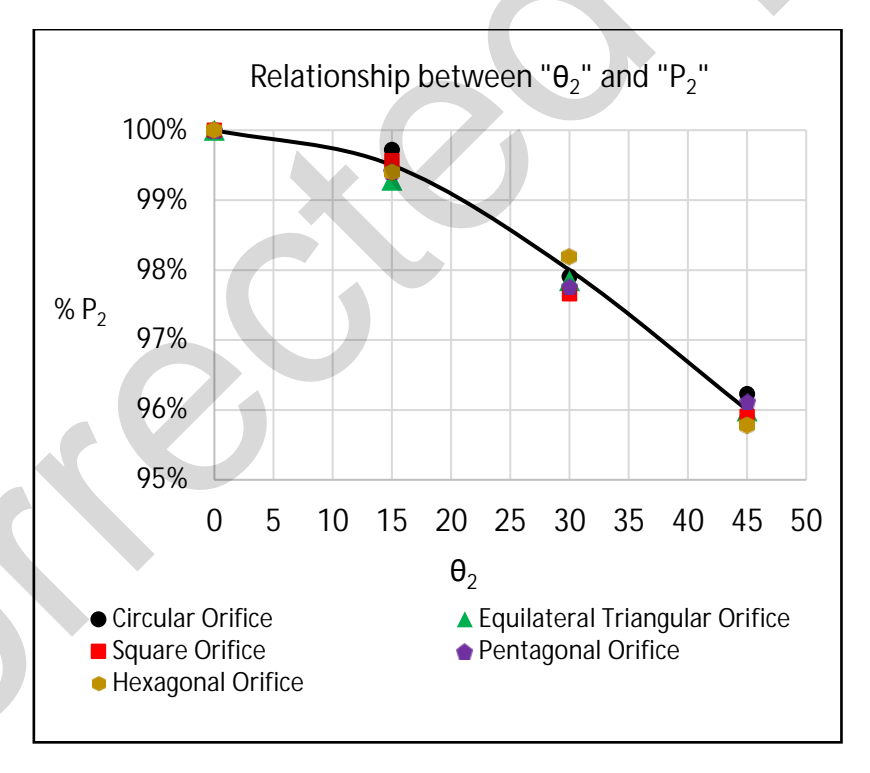


Fig. 12: Relationship between rotation angle (θ_2) and C_d reduction percentage (P_2) for different polygonal shapes.

The values of (P_2) oscillate around a maximum value of 92%, and varies by a maximum of 8%. This value varies based on the angle θ_2 , but does not depend on the number of polygon sides so a typical equation to describe the relationship between the angle (θ_2) and the percentage (P_2) is as follows:

$$P_2 = 0.96 + 0.04 \cos(2\theta_2)$$
 Eq. 19

The mathematical upper and lower bounds of the equation can be expressed as:

$$\lim_{\cos(m\theta_2)\to -1} (P_2) = 0.92$$
 Eq. 20

$$\lim_{\cos(m\theta_2)\to 1} (P_2) = 1$$
, where $P_2 \in [0.92, 1]$ Eq. 21

The following (**Fig. 13**) illustrates the extension of the curve completing a full cycle with a 360-degree angle.

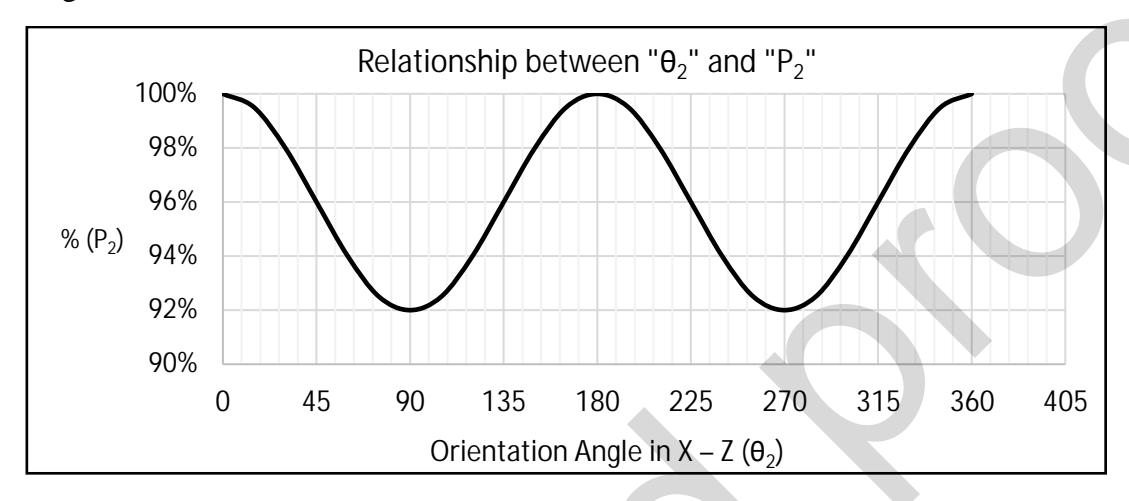


Fig. 13: Extended relationship between θ_2 and C_d reduction (P_2)

The effect of 3D inclination angles on the discharge coefficient for water flow through regular polygonal multi-orifice exits can be expressed using the combined percentages P₁ and P₂ as:

$$[C_d]_{\theta_1,\theta_2} = P_1 P_2 [C_d]_{0^{\circ},0^{\circ}}$$
 Eq. 22

$$[C_d]_{\theta_1,\theta_2} = [0.97 + 0.03\cos(m\theta_1)][0.96 + 0.04\cos(2\theta_2)][C_d]_{0^{\circ},0^{\circ}}$$
 Eq. 23

Where, $[C_d]_{\theta_1,\theta_2}$ is the discharge coefficient at θ_1 and θ_2 and $[C_d]_{0^\circ,0^\circ}$ is the discharge coefficient when both inclination angles are zero.

CONCLUSIONS AND RECOMMENDATIONS:

This study investigated the effect of 3D rotational angles, θ_1 (about the X-axis) and θ_2 (about the Y-axis), on discharge coefficients (C_d) in multi-orifice flow systems. The results demonstrated that circular orifices maintained the highest and most consistent C_d values (0.716-0.736), while polygonal shapes exhibited lower C_d values. For θ_1 rotation, experimental C_d values ranged from 0.637 to 0.685 for triangular, 0.616 to 0.684 for square, 0.630 to 0.670 for pentagonal, and 0.620 to 0.676 for hexagonal orifices. Comparative analysis between experimental measurements and CFD simulations showed strong agreement with maximum deviations of 4.5%. The study established that discharge coefficient variations follow cosine functions, quantified through percentage metrics P_1 and P_2 . P_1 varies with both rotation angle and the number of polygon sides (m), reaching a minimum of 94% of its original value with an amplitude of 6%. P_2 follows a consistent cosine pattern across all shapes, achieving a minimum of 92% of its original value with an amplitude of 8%, with a fixed periodicity of $2\theta_2$, reflecting the uniform behavior about the Y-axis rotation. For θ_2 rotation, all shapes showed similar behavior, with C_d values ranging from 0.689 - 0.716 for circular, 0.669 - 0.697 for triangular, 0.656-0.684 for square, 0.644 - 0.670 for pentagonal, and 0.636 - 0.664 for hexagonal orifices.

This study offers a clear understanding of how geometric factors affect discharge in multi-orifice systems, helping with better flow control. Future research could look into different orifice shapes, spacing, and more complex flow situations, using the strong link between experimental and CFD results.

REFERENCES

- [1] M. A. A. Alabas, "Evaluation of the hydraulic performance of drip irrigation system with multi cases," Glob. J. Res. Eng. Gen. Eng. 13(2), 13–18., 2013, [Online]. Available: https://cdnx.uobabylon.edu.iq/research/o3dUDJjInUKZj8yThtncpQ.pdf
- [2] M. Đurđević, M. Bukurov, S. Tašin, and S. Bikić, "Numerical study of single-hole and multi-holes orifice flow parameters," J. Appl. Fluid Mech., vol. 14, no. 1, pp. 215–226, 2021, doi: 10.47176/jafm.14.01.31472.
- [3] M. A. S. Wali, "Experimental analysis of multi-phase flows in orifice [Master's thesis, University of Stavanger]. University of Stavanger Open Research Repository.," 2022. [Online]. Available: https://uis.brage.unit.no/uis-xmlui/bitstream/handle/11250/3027386/no.uis:inspera:108215571:65744290.pdf
- [4] S. Huang, T. Ma, D. Wang, and Z. Lin, "Study on discharge coefficient of perforated orifices as a new kind of flowmeter," Exp. Therm. Fluid Sci., vol. 46, pp. 74–83, 2013, doi: 10.1016/j.expthermflusci.2012.11.022.
- [5] P. Khosravinia, M. R. Nikpour, O. Kisi, and R. M. Adnan, "Predicting discharge coefficient of triangular side orifice using LSSVM optimized by gravity search algorithm," Water (Switzerland), vol. 15, no. 7, pp. 1–18, 2023, doi: 10.3390/w15071341.
- [6] A. Mrowiec, "Uncertainty assessment for determining the discharge coefficient C for a multi-opening orifice," Appl. Sci., vol. 10, no. 23, pp. 1–10, 2020, doi: 10.3390/app10238503.
- [7] A. Golijanek-J, A. Mrowiec, R. Hanus, M. Zych, and M. Jaszczur, "A numerical and experimental analysis of multi-hole orifice in turbulent flow," Measurement, vol. 193, p. 110910, 2022, doi: 10.1016/j.measurement.2022.110910.
- [8] M. K. Babu and G. C. Gowda, "Discharge coefficient prediction for multi-hole orifice plate in a turbulent flow through pipe: Experimental and numerical investigation," Int. J. Eng. Res. Mech. Civ. Eng., vol. 2, no. 4, pp. 697–701, [Online]. Available: https://www.technoarete.org/common_abstract/pdf/IJERMCE/v4/i4/Ext_47615.pdf
- [9] J. Almutairi, A. Hasečić, and E. Džaferović, "Numerical analysis of Newtonian fluid flow through multi-hole orifice meter," in Proceedings of the 9th World Congress on Mechanical, Chemical, and Material Engineering (MCM'23), London: Brunel University, 2023, pp. 1–8. doi: 10.11159/htff23.182.
- [10] M. H. Assran, H. I. Mohamed, and B. Shenouda, "Effect of orifice-meter shape on discharge coefficient and head loss through it," Res. Sq., 2022, doi: 10.21203/rs.3.rs-1741688/v1.
- [11] M. H. Assran, B. Shenouda, and H. I. Mohamed, "Optimized orifice geometry to enhance the flow environment and achieve maximum discharge coefficient for effective water resources management," Aswan Univ. J. Environ. Stud., vol. 5, no. 2, pp. 142–163, 2024, doi: 10.21608/aujes.2024.272365.1216.